nuclear fusion
IAEA

PAPER • OPEN ACCESS

Tungsten impurity reduction by ICRH in a high power injection and high performance H-mode discharge on EAST

To cite this article: Zhen Zhou *et al* 2025 *Nucl. Fusion* **65** 036004

OPEN ACCESS
IOP Publishing | International Atomic Energy Agency
Nuclear Fusion
Nucl. Fusion **65** (2025) 036004 (10pp)
https://doi.org/10.1088/1741-4326/adafc4

Tungsten impurity reduction by ICRH in a high power injection and high performance H-mode discharge on EAST

Zhen Zhou[1,2], Shengyu Shi[2,3,*], Ling Zhang[2], Tao Zhang[2], Xiaohe Wu[1,2], Yunxin Cheng[2], Wenmin Zhang[1,2], Chaowei Mai[4], Shengyu Fu[1,2], Yifei Jin[1,2], Xiang Jian[2], Kaixuan Ye[2], Lin Yu[1,2], Ziqiang Zhou[1,2], Jiuyang Ma[1,2], Shuqi Yang[1,2], Kangning Geng[2], Gongshun Li[2], Jia Huang[2], Fei Wen[2], Yunfeng Liang[5] and Xiang Gao[2,*]

[1] University of Science and Technology of China, Hefei 230026, China
[2] Hefei Institutes of Physical Science, Chinese Academy of Sciences, Hefei 230031, China
[3] Oak Ridge Associated Universities, Oak Ridge, TN 37831, United States of America
[4] Guangdong Ocean University, Zhanjiang 524088, China
[5] Institute of Fusion Energy and Nuclear Waste Management - Plasmaphysik (IFN-1), Forschungszentrum Jülich GmbH, Jülich 52425, Germany

E-mail: syshi@ipp.ac.cn and xgao@ipp.ac.cn

Received 5 September 2024, revised 10 January 2025
Accepted for publication 29 January 2025
Published 10 February 2025

Abstract

The decrease in tungsten (W) content with the higher ion cyclotron resonance heating (ICRH) power is observed and explained for the first time in a high power injection ($P_{inj} > 10$ MW), high performance ($\beta_N \sim 2$, $\beta_P \sim 2.8$, $n_e/n_{GW} \sim 80\%$, $f_{BS} \sim 60\%$) H-mode discharge on experimental advanced superconducting tokamak. Unlike the previous phenomenon of electron cyclotron resonance heating core W control (Shi *et al* 2022 *Nucl. Fusion* **62** 066031), there is a slight change in the background plasma temperature when higher ICRH is applied, but the toroidal rotational velocity decreases by $\sim$10 km s^{-1} . Under this condition, the intensity of W unresolved transition array spectral structure in the region of 45–70 Å (which is composed of W^{27+}-W^{45+} line emissions) and W^{44+} density through spectroscopy in the Extreme Ultraviolet region decreases markedly. In addition, the poloidal asymmetry of radiation distribution from the tomographic inversions of Soft x-ray emission is reduced obviously. Theoretical modeling results indicate that the reduction in toroidal rotation leads to less W poloidal asymmetry and neoclassical pinch, which is more efficient in alleviating the core W accumulation than the improvement of isotropic hydrogen (H) minority temperature. The effects of isotropic and anisotropic H minority from ICRH on W transport are compared in the simulation lastly.

* Authors to whom any correspondence should be addressed.

Keywords: ICRH, W reduction, EAST, W neoclassical transport, H minority, isotropic and anisotropic effects

(Some figures may appear in colour only in the online journal)

1. Introduction

Due to the favorable properties such as high melting point, low tritium retention and low sputtering yield, tungsten (W) is selected as the plasma-facing components (PFCs) in the International Thermonuclear Experimental Reactor (ITER). Additionally, W is a candidate material for future fusion reactors and has been applied in many tokamaks such as JET [1], EAST [2], WEST [3–5] and ASDEX Upgrade (AUG) [6, 7]. Furthermore, DIII-D is also planning to update the PFCs with W as the frontrunner choices [8]. In particular, the first wall material of the ITER has been decided to change from light/low-Z Beryllium to W [9]. However, at thermonuclear fusion relevant temperature, non-fully ionized W can generate a very high line radiation, if they accumulate in the core region and the concentration exceeds a certain level, the plasma performance will be degraded significantly, even H to L-mode back transition and radiative collapse will also happen [10–12]. Consequently, understanding W transport and developing effective methods to control core W accumulation has become increasingly important for ensuring optimal plasma performance and stable operation in both present tokamaks and future fusion reactors. A quite promising method for core W control is on-axis electron cyclotron resonance heating (ECRH), which has been extensively studied in AUG, DIII-D and EAST [13–15]. Compared to ECRH scheme, ion cyclotron resonance heating (ICRH) offers additional advantages for core W control. ICRH not only can increase the temperature and its gradient thus changing the background plasma turbulent regime to enlarge the W turbulent diffusion coefficient [16], but also can decrease even reverse the inward neoclassical pinch [17–20] through (1) flatting the main ion density and rotation profile; (2) increasing the neoclassical temperature screening from main ion and fast ion; (3) reducing W poloidal asymmetry caused by toroidal rotation according to the parallel force balance. ICRH is also well-suited for central plasma heating under high density conditions due to there is no high density cut-off. These benefits of ICRH on core heavy impurities control are very attractive for EAST high performance operation. Currently, the PFCs of EAST are all metals, with upper and lower divertor covered by W and molybdenum (Mo) wall in the main chamber [21]. The counter current neutral beam injection (NBI) is also changed to co-NBI in EAST [22], when they are simultaneously applied in the high power injection experimental campaign, the increased toroidal rotation can produce a large centrifugal force (CF) for W, leading W poloidal distribution asymmetry, then enlarge W neoclassical portion, especially increase the inward neoclassical pinch, which may result in W accumulation [23–25].

However, in addition to generating fast waves for heating, the ICRH antennas can also excite a slow wave that corresponds to the parallel electric field [26–28]. The lighter electrons are easily accelerated by this parallel electric field and lose at PFCs surfaces, which leads to the formation of Radio-Frequency (RF) sheaths. Ions accelerated by RF sheaths cause a strong interaction with the PFCs along the magnetic field lines, which produces additional impurities sources in EAST [29] and WEST [30]. Fortunately, since 2020, EAST has modified the ICRH window and optimized the ICRH antennas [31, 32], and a significant reduction in W content by ICRH after these upgrades was first observed in a high power injection and high performance ($\beta_N \sim 2$, $\beta_P \sim 2.8$, $n_e/n_{GW} \sim 80\%$, $f_{BS} \sim 60\%$) H-mode discharge on EAST, which will be detailed in the section 2. The physics of decreased W content by ICRH will be illustrated in section 3. The discussions and conclusions will be given in sections 4 and 5 respectively.

2. Experimental observation of core W reduction by ICRH

High power injection and high performance regime with heavy metal material as the PFCs is the major goal for EAST to support ITER's scientific research. In order to achieve this goal, EAST has undertaken a series of upgrades as mentioned in the introduction, especially, the ICRH system optimization. The process is briefly described as follows: (1) The window of ICRH and 2.45 GHz LHW1 has been swapped to improve the heating efficiency of the 4.6 GHz LHW2 [32], which leads to a 30% reduction in the magnetic connection area between the 4.6 GHz LHW2 antennas and the ICRH antenna. In addition, the W source from LHW antennas sputtered by the ions accelerated by ICRH RF sheaths through magnetic connections may also be decreased. (2) The ICRH antennas themselves have also been improved. The main parameters of the new antennas are the lower $k_{\parallel}$ of the power spectrum, field aligned Faraday screen and two current strap configuration. With these upgrades, a high power injection ($P_{inj} > 10$ MW) and high performance ($\beta_N \sim 2$, $\beta_P \sim 2.8$, $n_e/n_{GW} \sim 80\%$, $f_{BS} \sim 60\%$) H-mode discharge is obtained successfully with low W content.

Time traces of this high performance discharge (shot #107838) are shown in figure 1. The toroidal magnetic field (B_T) and the plasma current (I_P) are ~2.3 T and 400 kA, respectively, with a double null divertor configuration. During 5.3–7.5 s, the 5.4 MW NBI, 2 MW LHW and 1.2 MW ECRH are almost kept constant. After 6.3 s, the ICRH power increases to 2.8 MW from 2 MW as shown in figure 1(*a*). The poloidal beta (β_P) and normalized beta (β_N) can be sustained

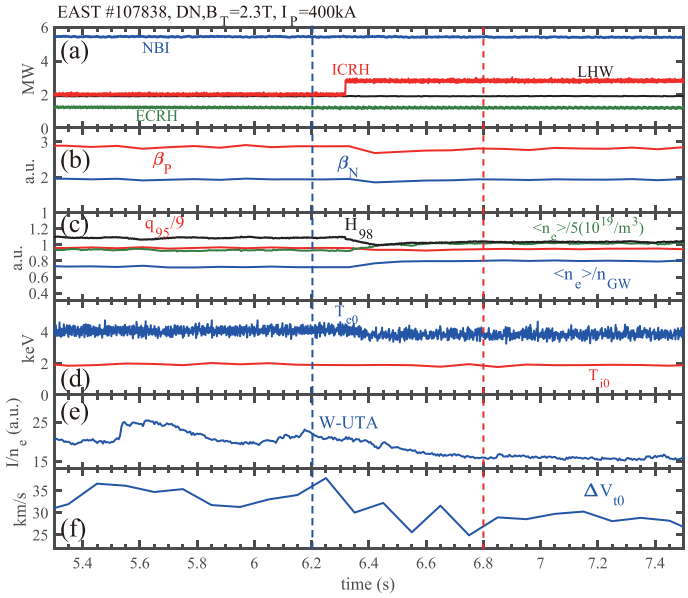

Figure 1. The time traces of (*a*) heating power, (*b*) plasma beta, (*c*) line-averaged density, Greenwald density fraction, q_{95} and H_{98}, (*d*) central electron and ion temperature, (*e*) intensity of W-UTA line normalized to electron density (*f*) central relative toroidal rotation velocity for EAST discharge 107 838.

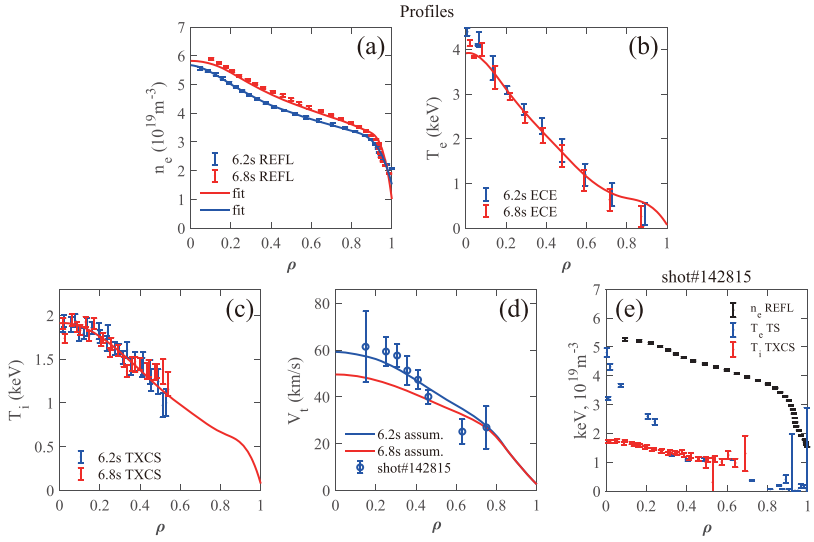

Figure 2. Kinetic profiles of (*a*) n_e measured by REFL, (*b*) T_e provided by ECE, (*c*) T_i diagnosed by TXCS, (*d*) V_t based on the TXCS and CXRS assumptions, (*e*) reference shot.

around 3 and 2, respectively, as shown in figure 1(*b*) with large $q_{95} \sim 9$, which leads to a high bootstrap current fraction ~60% as shown in figure 1(*c*). The other two key parameters for fusion energy, the plasma confinement factor $H_{98y2} \sim 1.1$ and Greenwald density fraction $f_{GW} \sim 0.8$ [33], also can be simultaneously maintained at a high level for EAST. Although this shot is mainly developed by NBI, the electron heating is still dominant (central electron temperature $T_{e0} \sim 4$ keV, ion temperature $T_{i0} \sim 2$ keV) as shown in figure 1(*d*), which is relevant to ITER research. When the ICRH is raised by only 0.8 MW (from 2 MW to 2.8 MW), the electron temperature profile measured by electron cyclotron emission (ECE) and the ion temperature profile measured by tokamak x-ray crystal spectroscopy (TXCS) showed little change, and the electron density profile measured by fast sweep frequency microwave reflectometer (REFL) increased slightly overall as shown in figure 2. Due to the lack of charge exchange recombination spectroscopy (CXRS) data, the toroidal rotation profile cannot be measured directly. The method of obtaining the toroidal rotation profile is as follows: The rotation profile before the application of higher power ICRH is assumed to be similar to that of shot#142 815, which has similar discharge conditions and CXRS data. The background plasma profile of shot#142 815 is shown in figure 2(*e*), where the electron temperature is obtained from the Thomson scattering (TS) diagnostic. Then based on the magnitude of the change

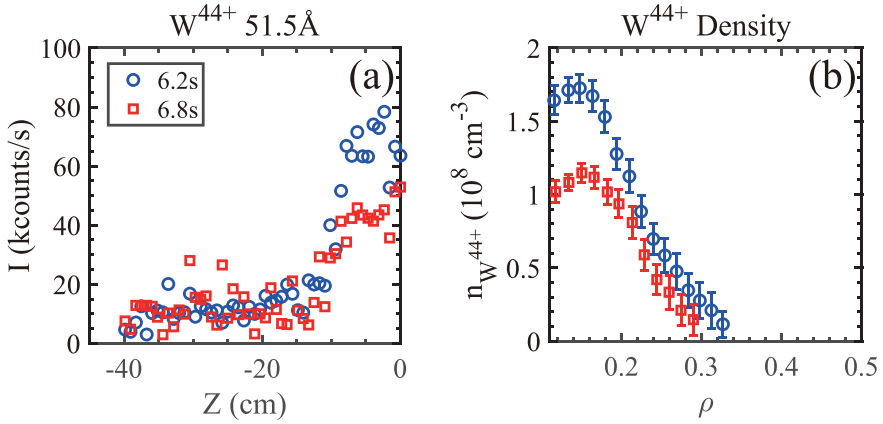

Figure 3. (*a*) Chord-integrated line intensity and (*b*) density distribution of W^{44+} measured by EUV.

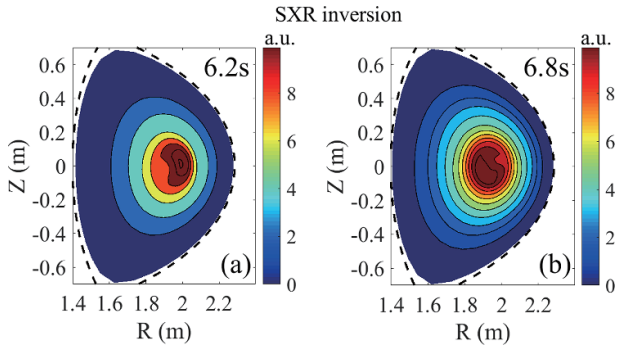

Figure 4. The tomographic inversions of SXR emission.

($\sim$10 km s^{-1}) in the relative rotation velocity provided by the TXCS as shown in figure 1(*f*), we can infer the toroidal rotation profiles with higher power ICRH. The intensity of W unresolved transition array (W-UTA) diagnosed by Extreme Ultra Violet (EUV) spectroscope [34] decreases by 20% as shown in figure 1(*e*). The intensity profiles of W^{44+} measured by EUV shows a reduction of more than 30% in the core, and the W^{44+} density profiles by EUV inversion also becomes less peaked as shown in figure 3. Although the central electron temperature decreased by approximately 5% as shown in figure 1(*d*), this would result in only $\sim$1% change in impurity density (the related analysis has been completed in [35]). However, the W^{44+} density has decreased by more than 30%, far exceeding the changes attributable to central electron temperature variations. In addition, the tomography from soft x-ray (SXR) diagnostics in figure 4 indicates that the radiation on the low-field side is stronger than that on the high-field side at $t = 6.2$ s, but the degree of the poloidal asymmetry decreases with higher ICRH power. It is well known that the poloidal asymmetry of impurities significantly affects their neoclassical transport. The smaller asymmetry can mitigate the core W accumulation [36, 37]. Therefore, core W content is reduced by ICRH in this high power injection and high performance H-mode discharge.

3. Theoretical modeling of ICRH core W alleviate

Theoretical modeling of ICRH core W alleviate is mainly performed by TRANSP [38] and TGYRO [39]. The TRANSP calculates the fast ion temperature distribution by invoking the TORIC [40] + FPP [41] code package. The temperature distribution of hydrogen (H) minority from ICRH is calculated by TRANSP assuming the H concentration of 6%. It is found that with the higher ICRH power, the effective temperature of the H minority ($T_{\rm eff} = [T_{\parallel} + 2\,T_{\perp}]/3$) at 6.8 s is much higher than that of 6.2 s as shown in figure 5. However, when the important role of the finite orbit width (FOW) effect is included [20], the H minority temperature profiles before and after addition ICRH applied are flatted as the FOW effect broadens fast ion orbits, increasing collisions with the background plasma, which significantly reduces the temperature distribution of fast ions. In this work, we will utilize the H minority temperature with the consideration of FOW to study the ICRH effects on the core W transport. In addition, the TRANSP modeling shows that the H minority resonance position is located at the high field side in figure 5(*c*), in this condition, we ignore the influence of the H minority anisotropy [20, 42], and only consider the effective temperature distribution on W transport because the NEO will overestimate the change in impurity asymmetry. Then the W transport coefficients are predicted by TGYRO, which calls TGLF [43–45] and NEO [46, 47] to calculate the turbulent and neoclassical transport, respectively. This method for the calculation of the W transport has been well explained in the [25, 48] and will not be detailed here. TGLF-SAT0 is used with electromagnetic effects in this modeling since the turbulence saturation amplitude coefficient of SAT0 has been calibrated with a large amount of data and has been thoroughly validated on EAST [15, 25, 31, 49–51]. The drift kinetic code NEO could compute the neoclassical transport component including the CF effects generated by toroidal rotation and ICRH H minority isotropic and anisotropic effects on the W neoclassical transport. A single W species with charge $Z = 44$ with trace level limit is considered here to model the core W transport [52] based on the electron

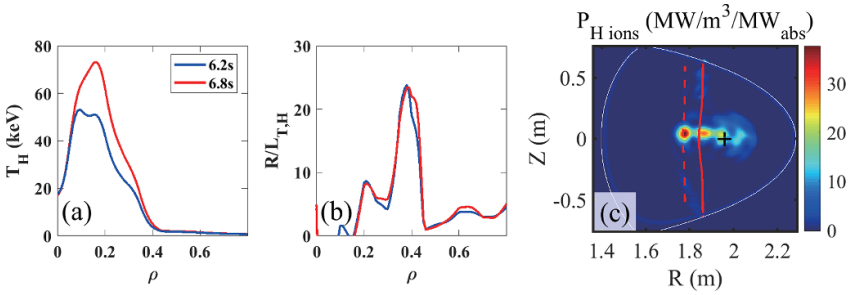

Figure 5. The distributions of (*a*) minority temperatures, (*b*) normalized minority temperature gradient and (*c*) minority heating power calculated by TRANSP. The solid red line in (*c*) is the cyclotron resonance layer of hydrogen, and the dashed line represents the ion-ion hybrid resonance position.

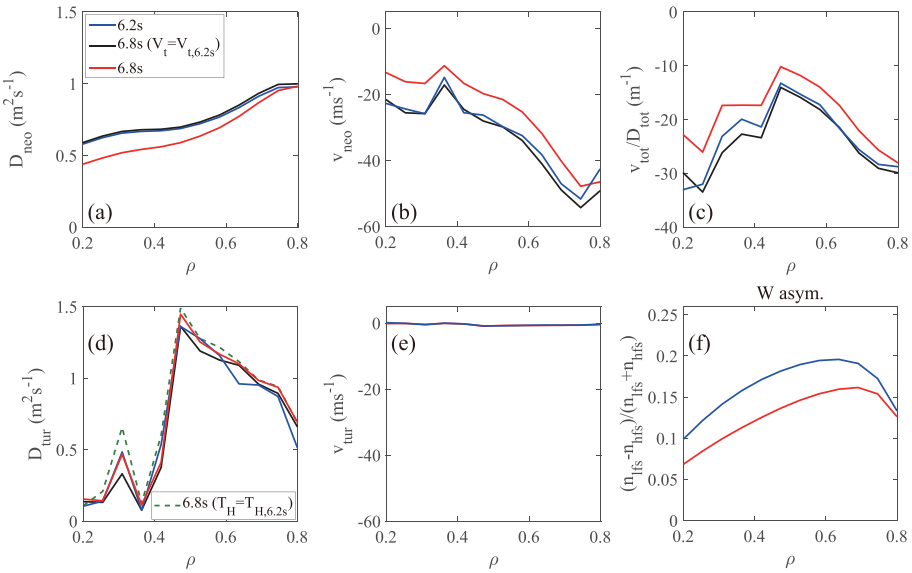

Figure 6. The distribution of (*a*)–(*e*) the neoclassical and turbulent transport coefficients calculated by NEO and TGLF respectively and (*f*) W poloidal asymmetry calculated by NEO.

temperature. Trace limit means that setting a very low impurity content, the plasma instability and turbulence are not affected by impurities and the transport of tungsten under trace limit conditions is determined by the background plasma.

The predicted W transport coefficients at $t = 6.2$ s in figure 6 show that the neoclassical diffusion coefficient is of the same order of magnitude as the turbulent one, but the turbulent convection can be ignored comparing the neoclassical one. The turbulent transport with negligible inward pinch and considerable diffusion coefficient is often conducive to the elimination of W if the W turbulent transport physics can be well captured by TGLF. On the contrary, the neoclassical inward pinch is very large, leading to a high W peaking factor. The W neoclassical pinch is caused by the main ion density gradient and can be enlarged by the toroidal rotation [25]. In the presence of toroidal rotation, W with large atomic mass could form a strong in-out asymmetric distribution in the poloidal direction produced by the CF, this asymmetry will enhance the inward neoclassical convection [37]. Therefore, at $t = 6.2$ s, the neoclassical inward convection is so strong that the total turbulent and neoclassical cannot compensate it, resulting in a large absolute value of $v_{\rm tot}/D_{\rm tot}$ as shown in figure 6(*c*).

In order to distinguish the effects of different parameters on the W transport, the black line in figure 6 considers all changes in the kinetic profiles, including the higher electron density and higher H minority isotropic temperature, while still using the rotation profile at $t = 6.2$ s. The red line further includes changes in the rotation profile. The results show that the higher H minority isotropic temperature cannot reduce the inward neoclassical pinch significantly and the inward neoclassical convection is slightly enhanced with higher electron density. However, when the decreased toroidal rotation is considered in the modeling, the poloidal asymmetry of W is reduced markedly so that neoclassical transport especially the neoclassical inward convection becomes much lower, leading to a less W peaking factor. To more intuitively illustrate the impact of rotation on the core tungsten impurity content, we statistics the relationship between $I_{\rm W\text{-}UTA}/n_{\rm e}$ and $V_{t,0}$ based on the data in figure 1. It should be noted that the rotation data is obtained by combining the relative data in figure 1 with the reference rotation data in figure 2, and the results

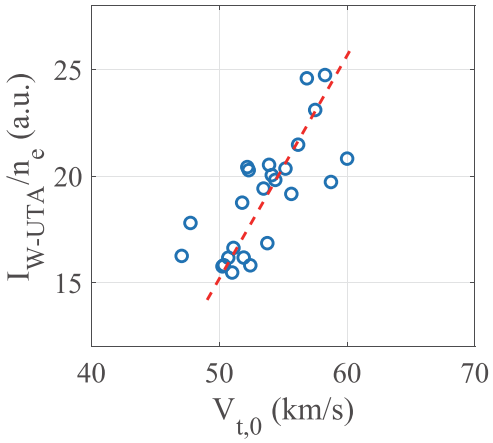

Figure 7. The $I_{\text{W-UTA}}/n_{\text{e}}$ as a function of $V_{t,0}$.

show that a significant dependence between the $I_{\text{W-UTA}}/n_{\text{e}}$ and rotation as shown in figure 7. An interesting phenomenon in figure 6(*d*) is that a slight decrease in D_{tur} ($\rho \sim 0.3$ and $\rho \sim 0.42$) can be observed at the locations where the ICRH fast ion temperature gradient increases in figure 5(*b*) as the ICRH power increases. To clearly illustrate the influence of fast ion on D_{tur}, we replaced the minority temperature profile at $t = 6.8$ s with that at $t = 6.2$ s, while keeping other background parameters unchanged. As shown in figure 6(*d*), the red solid line and green dashed line represent the original and modified minority temperature profile, respectively. The results show that the decrease of D_{tur} corresponds to the location of the enhanced normalized minority temperature gradient. Experimental and simulation results indicate that ICRH fast ions have a stabilizing effect on low-k turbulence (such as ITG and TEM) [53, 54], which plays a dominant role in impurity transport [55]. The interesting result in figure 6(*d*) may be related to Shafranov shift as it can be enhanced by larger fast ion temperature gradient with higher ICRH power, which is an important mechanism for turbulence stabilization considered by TGLF [56, 57]. It should be noted that the physical mechanisms by which fast ions influence turbulence not fully captured by TGLF, such as the non-linear interactions between fast ion modes, zonal flows and turbulence. However, since the ICRH power only increased from 2 MW to 2.8 MW in this work, the normalized temperature gradient growth of ICRH fast ion was limited, resulting in a relatively small effect on the turbulent transport of impurity. Therefore, ICRH can flat the W density profile and reduce the W content by decreasing the toroidal rotation in this high power injection and high performance H-mode discharge. ICRH-induced plasma toroidal rotation has been observed in multiple devices, such as TFTR [58], JET [59], and WEST [30]. However, the direction of ICRH-driven rotation is not uniform, it can be co-current or counter-current, depending on various factors such as ICRH resonance conditions, minority concentration, and antenna parameters. Currently, there is no unified theory to explain the behavior. On EAST, we observed that ICRH-driven plasma rotation is predominantly in the counter-current direction, including shot#107 838. Besides the ICRH-driven counter-current rotation, the influence of electron density on toroidal rotation has been observed in many tokamak experiments and the results suggest that higher densities may also contribute to the reduction of rotation [60, 61], but it is unclear which effect has the greater impact on rotation. This requires further investigation in future studies.

To illustrate the relationship between W impurity behavior and ICRH on EAST, we have statistically analyzed the degree of $I_{\text{W-UTA}}$ change at different ICRH power on EAST, where the positive and negative values indicate the degree of increase and decrease, respectively ($I_{\text{W-UTA}}$ change $= [I_{\text{W-UTA,t2}}/n_{\text{e,t2}} — I_{\text{W-UTA, t1}}/n_{\text{e,t1}}]/\ I_{\text{W-UTA,t1}}/n_{\text{e,t1}}$). Figure 8 shows that the content of tungsten increases with higher ICRH power because the RF sheath generated by ICRH enhances plasma-wall interactions, introducing additional impurity sources [29]. However, as the density increases, the growth rate of tungsten content decreases, probably because the RF sheath is dissipated at higher densities, contributing to the reduction of impurity sources. The increase in tungsten content is negative, accompanied by higher electron density in shot#107 838. For core transport, higher electron density does not reduce the $v_{\text{tot}}/D_{\text{tot}}$, as shown in figure 6(*c*). On the other hand, the Fe^{4+} content, primarily located in the extreme edge region, shows little change in figure 10. In the absence of experimental data from W source, the trend of Fe^{4+} can be regarded as the trend of W source. Therefore, the significant reduction in tungsten content is related to other factors. In the current analysis, we attribute this to the reduction in plasma rotation. This is supported by the statistical data on $I_{\text{W-UTA}}/n_{\text{e}}$ and $V_{t,0}$, which indicate a significant dependence between $I_{\text{W-UTA}}/n_{\text{e}}$ and rotation. Additionally, ICRH also causes a reduction in plasma toroidal rotation, as shown in figure 8(*b*). The electron density in shot#107 838 is higher than the blue and red data points in figure 8(*a*), and the rotation reduction is also larger than the trend in figure 8(*b*). Consequently, the increase in tungsten content becomes negative, as indicated by the pentagram data point in figure 8(*a*).

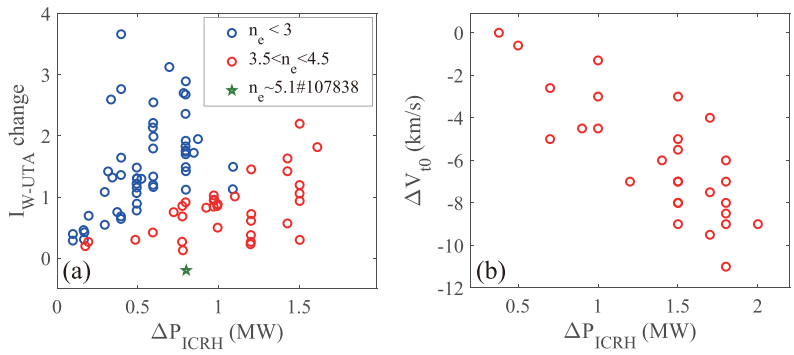

Figure 8. The dependence of $I_{\text{W-UTA}}$ change and rotation change on ICRH power.

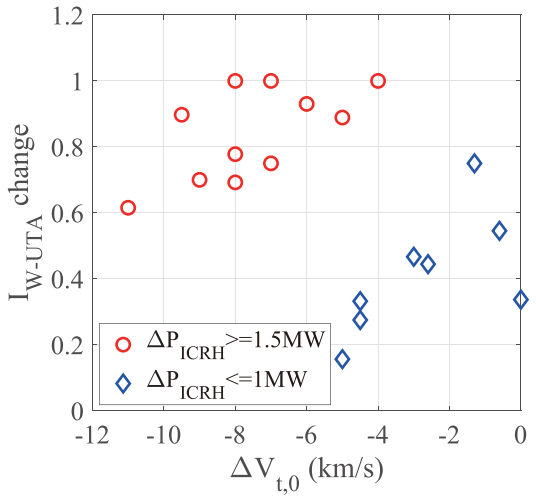

Figure 9. The dependence of $I_{\text{W-UTA}}$ change on $\Delta V_{t,0}$.

In addition, based on the data in figure 8(*b*), we further satisficed the relationship between $I_{\text{W-UTA}}$ change and $\Delta V_{t,0}$. The results in figure 9 show two distinct branches, corresponding to different ICRH power levels. Although higher ICRH power results in a larger increase in tungsten content, both branches appear to follow a similar trend: the greater the reduction in rotation, the smaller the increase in tungsten content. This result suggests that rotation changes induced by ICRH have a significant impact on the behavior of W impurities.

4. Discussions

The decrease of tungsten content with higher power ICRH may be related to multiple factors in shot#107 838. In addition to the ICRH antenna upgrades mentioned in sections 1 and 2, first, the well lithiated wall environment may control the W source. It may also be related to the higher electron density, which helps ICRH coupling. As shown in figure 10, after additional ICRH is applied, the contents of Li^{2+} and C^{5+} slight increased but there is no significant change in Fe^{4+}, which mainly exists in the extreme edge region. Therefore, in shot#107 838, ICRH may not introduce additional W source as the previous EAST and WEST experiments [28, 29], which may be the one of the important reasons for ICRH W alleviate. It should be noted that although the collision transport between light impurities and W is generally not considered in this work, light impurities may still indirectly influence the behavior of core W.

In fact, the fast ion also has a significant impact on the transport of W impurities, which can enhance the neoclassical temperature screening effect, thereby mitigating the accumulation of W impurities in the core. Based on the kinetic profiles at $t = 6.2$ s, we evaluate the effect of increasing the ICRH power from 2 MW to 2.8 MW on the neoclassical screening effect by adjusting the fast ion temperature in figure 11. The FOW effect broadens fast ion orbits, increasing collisions with the background plasma, which significantly reduces the temperature distribution of fast ion as shown in figures 11(*a*) and 5(*a*). Regardless of whether the FOW effect is considered, the location where the normalized temperature gradient of fast ion increases corresponds to a reduction in the inward neoclassical convection, indicating that the temperature screening effect of fast ion also plays an important role. However, due to the limited increase in ICRH power, its impact on neoclassical transport is not as substantial as the effect of rotational changes.

As mentioned in the section 3, ICRH enables core W alleviate by reducing the toroidal rotation. However, the rotation direction driven by ICRH is related to many factors, and there is no unified theoretical explanation. Therefore, this method of alleviating W by ICRH reducing the toroidal rotation may become difficult, a more general and effective approach is needed. In this work, since the ICRH resonance location is on the high filed side, only the H minority isotropic effects are considered, indicating that a 0.8 MW increase in ICRH power does not significantly affect W transport. However, if resonance position of the ICRH can be changed from the high field side to the low field side in EAST, ICRH is likely to achieve more efficient control of W by increasing the H minority temperature anisotropy. We import the perpendicular and parallel temperatures of the minority into NEO to assess the impact of minority anisotropy on the W transport. The perpendicular temperature, parallel temperatures and the magnitude of H minority anisotropy represented by the ratio of perpendicular temperature to parallel temperature at $t = 6.2$ s and $t = 6.8$ s are calculated by TRANSP and shown in figures 12(*a*) and (*b*). Compared to the isotropic effect the

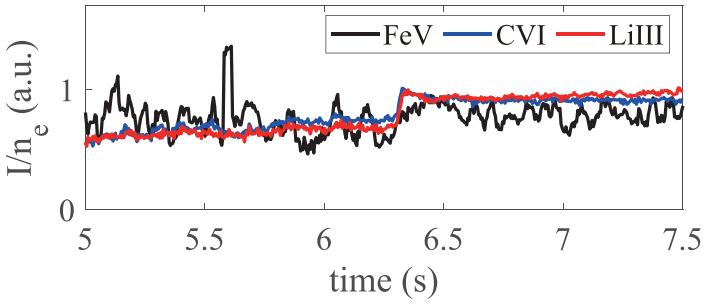

Figure 10. The time traces of contents of Li^{2+}, C^{5+} and Fe^{4+} measured by EUV for EAST discharge 107 838.

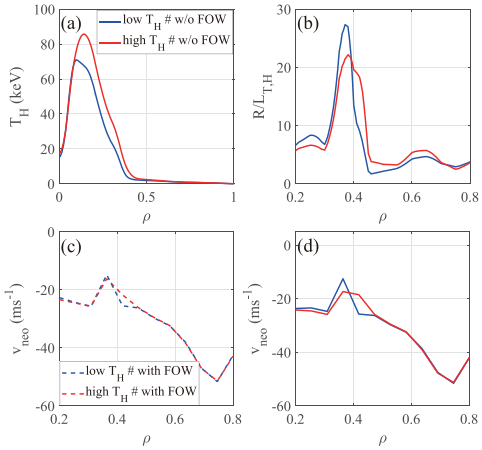

Figure 11. The distribution of (*a*) minority temperatures, (*b*) normalized minority temperature gradient without FOW, neoclassical convection with (*c*) and without (*d*) FOW respectively.

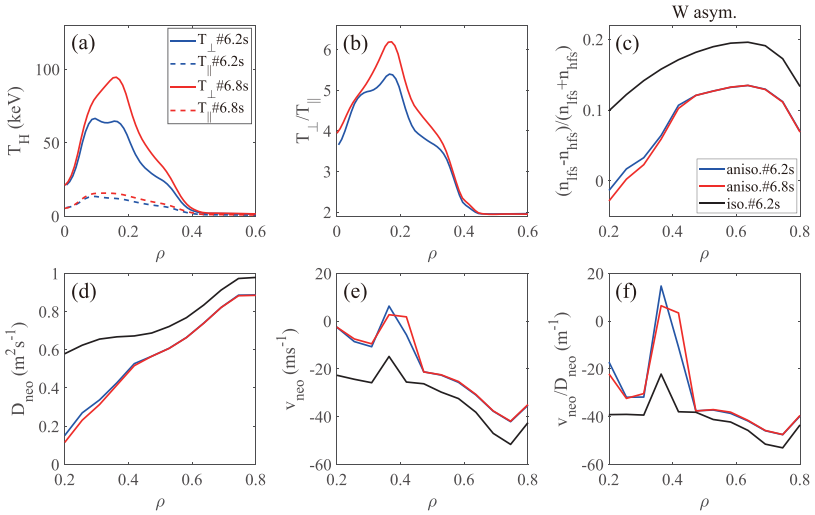

Figure 12. The distribution of (*a*) perpendicular and parallel temperatures of the minority, (*b*) anisotropy magnitude of the minority, (*c*) W poloidal asymmetry, (*d*)–(*f*) the neoclassical transport coefficient.

additional ICRH could enlarge the magnitude of H minority anisotropy. In this condition, the W poloidal asymmetry and inward neoclassical convection are effectively reduced as shown in figure 12. Although the W neoclassical diffusion coefficient also decreases, the reduction in neoclassical convection is more significant, resulting in a smaller absolute value of $v_{\rm neo}/D_{\rm neo}$, which greatly contributes to alleviating the accumulation of W in the core region. The physical explanation of the ICRH H minority anisotropic effect on the W transport is that the anisotropic minority species with $T_\perp > T_\parallel$ can produce a poloidal electric field [18, 42] and this field can push heavy impurities towards HFS to counteract (partially) the effects of CF through parallel force balance equation, leading to the decreases of the neoclassical component especially

for the neoclassical convection velocity. After ICRH increased by 0.8 MW, the neoclassical convection reversed in more locations. Therefore, it is well worth for EAST investigating how to experimentally realize the low field side resonance of ICRH and the effects of ICRH of low field side resonance on the W transport in the future.

5. Conclusions

The behavior of W in a high-power injection ($P_{\mathrm{inj}} > 10$ MW) and high beta ($\beta_{\mathrm{N}} \sim 2$, $\beta_{\mathrm{P}} \sim 2.8$) discharge with Li-coated walls on EAST is analyzed. It is found that the W content is reduced with higher ICRH power injection. The experimental diagnosis shows that the plasma temperature profile does not change much, but the core rotation is reduced by $\sim$10 km s^{-1}. The difference from the previous results on EAST may be related to several factors. The optimization of the ICRH antenna and the swapping of the ICRH window were important prerequisites. The high density and well lithiated wall discharge conditions ensured effective control of the impurity sources. Finally, the effect of asymmetry in the W impurity distribution on impurity transport could be observed. The simulation analysis found that the inward neoclassical convection enhanced by the tungsten poloidal asymmetry caused by the rotation effect leads to the peak tungsten density distribution. With the reduction of rotation, the poloidal asymmetry is alleviated, and the inward neoclassical convection is significantly reduced, which is conducive to alleviating the accumulation of tungsten impurities in the core. The reduction in asymmetry is confirmed by the SXR tomographic inversions. Compared with rotation reduction, the change of H minority isotropic temperature has little effect on the W transport for 0.8 MW power increase in ICRH.

Although ICRH helps to reduce the toroidal rotation, the similar phenomenon has not been observed in all devices, and the underlying physical reasons remain to be studied. Therefore, it is meaningful to explore a more effective method. The simulations indicate that the minority anisotropy has a more significant impact on W impurity transport, but the effect requires the ICRH resonance position is located at the low field side. However, the ICRH resonance is often located on the high field side and near the magnetic axis on EAST. Therefore, the effect of ICRH on W impurity transport under different ICRH resonance conditions will be a key focus for the future research.

Acknowledgment

We would like to warmly thank Dr Francis Casson and Dr Patrick Maget for very helpful discussions and the scientists and maintainers who developed TRANSP. In addition, we sincerely acknowledges the General Atomics Theory Group for permission to use the OMFIT framework and GA code suite. Numerical computations were performed on the Shen Ma High Performance Computing Cluster in the Institute of Plasma Physics, Chinese Academy of Sciences. This work is mainly supported by the fellowship of china national postdoctoral program for talents under BX20220304, and the U.S. Department of Energy, Office of Science, Office of Fusion Energy Sciences, under Award DE-SC0010685 and DE-FC02-04ER54698, and the National Natural Science Foundation of China (No. 12175277), and the National Key R&D Program of China under Contract No. 2022YFE03050003 and the Open Fund of Magnetic Confinement Laboratory of Anhui Province (No. 2023AMF03005), the National Natural Science Foundation of China (No. 12405271).

ORCID iDs

Zhen Zhou https://orcid.org/0009-0000-8261-7837
Tao Zhang https://orcid.org/0000-0002-1555-6226
Yunxin Cheng https://orcid.org/0000-0002-9195-2757
Wenmin Zhang https://orcid.org/0009-0000-9980-6765
Chaowei Mai https://orcid.org/0000-0001-9981-2620
Yifei Jin https://orcid.org/0000-0002-3061-6709
Xiang Jian https://orcid.org/0000-0003-3052-1694
Kaixuan Ye https://orcid.org/0000-0003-0927-4502
Lin Yu https://orcid.org/0009-0004-1339-2389
Kangning Geng https://orcid.org/0000-0001-7808-0192
Gongshun Li https://orcid.org/0000-0002-5542-1238
Jia Huang https://orcid.org/0000-0001-6289-1812
Xiang Gao https://orcid.org/0000-0003-1885-2538

References

[1] Mathews G.F. *et al* 2013 *J. Nucl. Mater.* **438** S2–S10
[2] Luo G.N. *et al* 2017 *Nucl. Fusion* **57** 065001
[3] Bucalossi J. *et al* 2014 *Fusion Eng. Des.* **89** 907–12
[4] Bourdelle C. *et al* 2015 *Nucl. Fusion* **55** 063017
[5] Richou M. *et al* 2015 *Fusion Eng. Des.* **98–99** 1394–8
[6] Neu R., Dux R., Geier A., Gruber O., Kallenbach A., Krieger K., Maier H., Pugno R., Rohde V. and Schweizer S. 2003 *Fusion Eng. Des.* **65** 367–74
[7] Neu R. *et al* 2009 *Phys. Scr.* **T138** 014038
[8] Abrams T. *et al* 2021 *Phys. Scr.* **96** 124073
[9] Ipatova I., Greaves G., Terentyev D., Gilbert M.R. and Chiu Y.-L. 2024 *Nucl. Eng. Technol.* **56** 1490–500
[10] de Vries P.C. *et al* 2014 *Phys. Plasmas* **21** 056101
[11] Loarte A., Koechl F., Leyland M.J., Polevoi A., Beurskens M., Parail V., Nunes I., Saibene G.R. and Sartori R.I.A. 2014 *Nucl. Fusion* **54** 123014
[12] Kochl F. *et al* 2018 *Plasma Phys. Control. Fusion* **60** 074008
[13] Dux R., Neu R., Peeters A.G., Pereverzev G., M Ck A., Ryter F. and Stober J. (ASDEX Upgrade Team) 2003 *Plasma Phys. Control. Fusion* **45** 1815–25
[14] Odstrcil T., Howard N.T., Sciortino F., Chrystal C., Holland C., Hollmann E., McKee G., Thome K.E. and Wilks T.M. 2020 *Phys. Plasmas* **27** 082503
[15] Shi S.Y. *et al* 2022 *Nucl. Fusion* **62** 066031
[16] Sertoli M., Angioni C. and Odstrcil T. 2017 *Phys. Plasmas* **24** 112503
[17] Angioni C., Sertoli M., Bilato R., Bobkov V., Loarte A., Ochoukov R., Odstrcil T., Pütterich T. and Stober J. 2017 *Nucl. Fusion* **57** 056015
[18] Casson F.J. *et al* 2015 *Plasma Phys. Control. Fusion* **57** 014031
[19] Rice J.E. *et al* 2002 *Nucl. Fusion* **42** 510
[20] Casson F.J. *et al* 2020 *Nucl. Fusion* **60** 066029
[21] Li J. and Wan Y. 2021 *Engineering* **7** 1523–8

[22] Xie Y.H. *et al* 2022 *IEEE Trans. Plasma Sci.* **50** 4086–90
[23] Angioni C. *et al* 2014 *Nucl. Fusion* **54** 083028
[24] Odstrcil T., Pütterich T., Angioni C., Bilato R., Gude A. and Odstrcil M. 2018 *Plasma Phys. Control. Fusion* **60** 014003
[25] Shi S.Y. *et al* 2022 *Nucl. Fusion* **62** 066032
[26] Zhang W. *et al* 2024 *Nucl. Fusion* **64** 096011
[27] Noterdaeme J.M. 1992 *AIP Conf. Proc.* **244** 71–87
[28] Urbanczyk G. *et al* 2020 *AIP Conf. Proc.* **2254** 030012
[29] Urbanczyk G. *et al* 2020 *Nucl. Fusion* **60** 126003
[30] Maget P. *et al* 2023 *Plasma Phys. Control. Fusion* **65** 125009
[31] Huang J. *et al* 2023 *Phys. Plasmas* **30** 062504
[32] Wang M. *et al* 2022 *Nucl. Eng. Technol.* **54** 4102–10
[33] Ding S. *et al* 2024 *Nature* **629** 555–60
[34] Zhang W.M. *et al* 2024 *Phys. Scr.* **99** 105609
[35] Cheng Y.X. *et al* 2022 *IEEE Trans. Plasma Sci.* **50** 691–9
[36] Romanelli M. and Ottaviani M. 1998 *Plasma Phys. Control. Fusion* **40** 1767
[37] Mochinaga S., Kasuya N., Fukuyama A. and Yagi M. 2024 *Nucl. Fusion* **64** 066002
[38] Breslau J., Gorelenkova M., Poli F., Sachdev J., Pankin A., Perumpilly G., Yuan X. and Glant L. 2018 *TRANSP* (https://doi.org/10.11578/dc.20180627.4) (Accessed 27 June 2018)
[39] Candy J., Holland C., Waltz R.E., Fahey M.R. and Belli E. 2009 *Phys. Plasmas* **16** 060704
[40] Brambilla M. *et al* 1999 *Plasma Phys. Control. Fusion* **41** 1–34
[41] Hammett G.W. 1986 Fast ion studies of ion cyclotron heating in the PLT tokamak *PhD Thesis* Princeton University PhD (Thesis Princeton University) Princeton
[42] Bilato R., Odstrcil T., Casson F.J., Angioni C., Brambilla M., Kazakov Y.O. and Poli E. 2017 *Nucl. Fusion* **57** 056020
[43] Staebler G.M., Howard N.T., Candy J. and Holland C. 2017 *Nucl. Fusion* **57** 066046
[44] Kinsey J.E., Staebler G.M. and Waltz R.E. 2008 *Phys. Plasmas* **15** 055908
[45] Staebler G., Kinsey J.E. and Waltz R.E. 2005 *Phys. Plasmas* **12** 102508
[46] Belli E.A. and Candy J. 2008 *Plasma Phys. Control. Fusion* **50** 095010
[47] Belli E.A. and Candy J. 2012 *Plasma Phys. Control. Fusion* **54** 015015
[48] Meneghini O. *et al* 2021 *Nucl. Fusion* **61** 026006
[49] Wu M.Q. *et al* 2019 *Nucl. Fusion* **59** 106009
[50] Shi S.Y., Chen J., Bourdelle C., Jian X., Wu M., Zhang T., Qian J., Garofalo A.M., Gao X. and Wan Y. 2021 *Nucl. Fusion* **61** 126055
[51] Nan K.B. *et al* 2024 *Plasma Phys. Control. Fusion* **66** 115015
[52] Fülöp T. and Nordman H. 2009 *Phys. Plasmas* **16** 032306
[53] Di Siena A., Görler T., Poli E., Navarro A.B., Biancalani A. and Jenko F. 2019 *Nucl. Fusion* **59** 124001
[54] Bonanomi N., Mantica P., Di Siena A., Delabie E., Giroud C., Johnson T., Lerche E., Menmuir S., Tsalas M. and Van Eester D. 2018 *Nucl. Fusion* **58** 056025
[55] García-Regaña J.M. *et al* 2021 *J. Plasma Phys.* **87** 855870103
[56] Beer M.A., Hammett G.W., Rewoldt G., Synakowski E.J., Zarnstorff M.C. and Dorland W. 1997 *Phys. Plasmas* **4** 1792–9
[57] Jian X., Chan V.S., Chen J., Bock A., Zohm H., Fable E., Reisner M., Guo W. and Zhuang G. 2019 *Nucl. Fusion* **59** 106038
[58] Chang C.S., Phillips C.K., White R., Zweben S., Bonoli P.T., Rice J.E., Greenwald M.J. and deGrassie J. 1999 *Phys. Plasmas* **6** 1969–77
[59] Eriksson L.G., Giannella R., Hellsten T., Kallne E. and Sundstrom G. 1992 *Plasma Phys. Control. Fusion* **34** 863
[60] Scarabosio A., Bortolon A., Duval B.P., Karpushov A. and Pochelon A. 2006 *Plasma Phys. Control. Fusion* **48** 663
[61] Brau K., Bitter M., Goldston R.J., Manos D., McGuire K. and Suckewer S. 1983 *Nucl. Fusion* **23** 1643